OPEN

NPG Asia Materials (2015) 7, e195; doi:10.1038/am.2015.63

www.nature.com/am

ORIGINAL ARTICLE

Three-dimensional-networked $NiCo_2S_4$ nanosheet array/carbon cloth anodes for high-performance lithium-ion batteries

Rujia Zou[1,2], Zhenyu Zhang[1], Muk Fung Yuen[1], Mingliang Sun[1], Junqing Hu[2], Chun-Sing Lee[1] and Wenjun Zhang[1]

We present the design and synthesis of three-dimensional (3D)-networked $NiCo_2S_4$ nanosheet arrays (NSAs) grown on carbon cloth along with their novel application as anodes in lithium-ion batteries. The relatively small (~60%) volumetric expansion of $NiCo_2S_4$ nanosheets during the lithiation process was confirmed by *in situ* transmission electron microscopy and is attributed to their mesoporous nature. The 3D network structure of $NiCo_2S_4$ nanosheets offers the additional advantages of large surface area, efficient electron and ion transport capability, easy access of electrolyte to the electrode surface, sufficient void space and mechanical robustness. The fabricated electrodes exhibited outstanding lithium-storage performance including high specific capacity, excellent cycling stability and high rate of performance. A reversible capacity of ~ 1275 mAh g^{-1} was obtained at a current density of 1000 mA g^{-1}, and the devices retained ~ 1137 mAh g^{-1} after 100 cycles, which is the highest value reported to date for electrodes made of metal sulfide nanostructures or their composites. Our results suggest that 3D-networked $NiCo_2S_4$ NSA/carbon cloth composites are a promising material for electrodes in high-performance lithium-ion batteries.
NPG Asia Materials (2015) **7,** e195; doi:10.1038/am.2015.63; published online 26 June 2015

INTRODUCTION

Rechargeable lithium-ion batteries (LIBs) are the most widely used electrochemical energy storage devices because of their inherent advantages including high energy density, long life span, lack of memory effect and environmental nontoxicity.[1–3] The increasing applications of LIBs in daily electronic devices—along with industry demands for further improvement in energy density, durability, rate capability and safety—have driven the development of new electrode materials and new electrode structures.[4–7] Among the great variety of anode materials studied, metal oxides (MOs) and metal sulfides (MSs) such as Co_3O_4,[8] SnO_2,[9] Fe_3O_4,[10] V_2O_5,[11] FeS_2,[12] NiS_2,[13] MoS_2[14] and WS_2 [15] comprise an important class of materials that can be charged and discharged through redox reactions. Compared with their MO counterparts, MSs generally feature higher electrical conductivity, better mechanical and thermal stability, and richer redox chemistry, making them attractive anode materials for high-performance LIBs.[16,17] Various MS nanostructures including nanoparticles,[18] nanosheets,[19] nanowires,[20] and nanotubes[21] have been synthesized and offer superior electrochemical energy storage capacity compared with bulk MSs. However, the large volumetric change of MS nanostructures during electrochemical reactions leads to reduced capacity and poor cycling stability. Moreover, the necessary addition of conductive additives and binders inevitably lessens overall energy storage capacity, and binders in particular hinder electron transport from MS nanostructures to the electron collector, limiting their practical applications.[16,17]

Recently, direct growth of self-supported $NiCo_2O_4$ nanowires and $ZnCo_2O_4$ nanowire arrays on current-collecting substrates has been shown to overcome the drawbacks of mixing active electrode materials with conductive additives and binders and to increase endurance of fast charge and discharge processes.[22,23] Furthermore, it has been reported that 3D network structures (for example, graphene networks,[7] MO/3D graphene network composites[24] and diamond/carbon nanotubes[25]) can provide open channels for efficient electron/ion transport and large surface area for reactions, both of which are favorable properties for materials and devices used in electrochemical applications. In this work, we report the synthesis of 3D-networked $NiCo_2S_4$ nanosheet arrays (NSAs) directly on carbon cloth and their application as an anode material in LIBs; to our knowledge, this is the first such demonstration. $NiCo_2S_4$ possesses an electric conductivity ~ 10^4 times higher than conventional MO semiconductors.[26] In previous studies, $NiCo_2S_4$ was shown to have outstanding electrochemical characteristics when used as an electrode material in supercapacitors.[27,28] Our work demonstrates that the direct growth of $NiCo_2S_4$ NSAs on carbon cloth enables their use as anodes in LIBs without requiring the addition of carbon additives and binders. *In situ*

[1]Center of Super-Diamond and Advanced Films (COSDAF), Department of Physics and Materials Science, City University of Hong Kong, Hong Kong, China and [2]State Key Laboratory for Modification of Chemical Fibers and Polymer Materials, College of Materials Science and Engineering, Donghua University, Shanghai, China
Correspondence: Professor J Hu or Professor W Zhang, Center of Super-Diamond and Advanced Films (COSDAF), Department Physics & Materials Science, City University of Hong Kong, Tat Chee Avenue, Kowloon Tong, Kowloon, Hong Kong, Hong Kong.
E-mail: hu.junqing@dhu.edu.cn or apwjzh@cityu.edu.hk
Received 21 December 2014; revised 19 March 2015; accepted 27 April 2015

transmission electron microscopy (TEM) observations verify that the volumetric expansion of $NiCo_2S_4$ nanosheets during the lithiation process is relatively small (~60%) as a result of their mesoporous nature. $NiCo_2S_4$ NSA/carbon cloth electrodes exhibit remarkable lithium storage properties that include the highest specific capacity for MS electrodes reported thus far (~1275 mAh g^{-1} at a current density of 1000 mA g^{-1}), excellent cycling stability (~89% retention after 100 cycles) and high rate capability, suggesting that it is a favorable anode material for high-performance LIBs.

MATERIALS AND METHODS

Synthesis

All chemicals used in this work are commercially available from Sigma-Aldrich (Shanghai, China) and were used as received without further purification. The 3D-networked $NiCo_2S_4$ NSAs were synthesized on carbon cloth using a hydrothermal reaction combined with a simple subsequent sulfurization process, as described in Supplementary Information I.

Characterization

Sample morphology and microstructure were characterized by scanning electron microscopy (Philips XL 30FEG, Amsterdam, Netherlands) and TEM (JEM-2100F equipped with an energy-dispersive X-ray spectrometer, Tokyo, Japan). X-ray diffraction patterns were recorded using a Philips X'Pert MRD X-ray diffractometer with Cu K_α radiation (Amsterdam, Netherlands). *In situ* TEM observation of the lithiation process was performed using a scanning tunneling microscopy-TEM holder from Nanofactory Instruments AB (Gothenburg, Sweden) within the JEOL 2100F TEM, which was operated at 200 kV.

Electrochemical measurements

The 3D-networked $NiCo_2S_4$ NSA/carbon cloth composites were used as working electrodes without adding any ancillary materials. The loading density of the $NiCo_2S_4$ NSAs (that is, the active material) was calculated to be 1.02–1.36 ± 4% mg. To allow electrochemical measurements of the control sample, the working electrode was prepared by mixing the $NiCo_2S_4$ flowers, conductive agent (carbon black) and binder (sodium alginate) in a weight ratio of 70:20:10. Coin-type cells (CR2032) were fabricated using lithium metal as the counter electrode, Celgard 2400 (Charlotte, NC, USA) as the separator and $LiPF_6$ (1 M) in ethylene carbonate-dimethyl carbonate (1:1 vol%) as the electrolyte. Cyclic voltammetry (CV) measurements were conducted at 0.1 mV s^{-1} over the range of 0.01–3.0 V (vs Li/Li^+) on a CHI 600D (Shanghai, China) electrochemical workstation. Electrochemical impedance spectroscopy was carried out with a ZAHNERelektrik IM 6 (Kronach, Germany) electrochemical system over a frequency range of 100 kHz to 0.01 Hz.

RESULTS AND DISCUSSION

The 3D-networked $NiCo_2S_4$ NSAs were synthesized by a two-step process as schematically illustrated in Figure 1a. In the first step, strips of carbon cloth (Supplementary Figure S1) were immersed into an aqueous solution containing Ni^{2+}, Co^{2+} and methenamine, and NiCo precursor nanosheets arrays were grown uniformly on the surface of the cloth, as shown in Supplementary Figure S2. In the second step, the NiCo precursor NSAs were converted to 3D-networked and mesoporous $NiCo_2S_4$ NSAs with well-retained morphology via a simple sulfurization treatment, and densely packed, highly ordered $NiCo_2S_4$ NSAs were formed on the cloth, as shown in Figures 1b and c. $NiCo_2S_4$ NSAs uniformly covered the entire surface of the carbon cloth, as depicted in the low-magnification scanning electron microcopy image shown in Figure 1b. Close observation (Figure 1d) revealed that the nanosheets were interconnected and intersected each other to form a 3D network structure with voids clearly observed (marked by red arrows) that was similar to the structure of sponge. The retention of the NiCo interconnected structure during sulfurization can be attributed to the robust support of the carbon cloth and the slow sulfurization rate at the relatively low temperature. This 3D network structure is concluded to be superior for use in LIB anodes because (1) it provides better mechanical strength and excellent transport properties for both Li^+ ions and electrons[24,25] and (2) the abundant empty space between the nanosheets may promote electrolyte penetration, facilitating the lithiation and delithiation of electrodes.[6,29] Moreover, $NiCo_2S_4$ NSAs are ultrathin (~10-nm thick), which greatly increases the specific surface area and promotes electrochemical reactions between electrode and electrolyte. Figure 1e presents the X-ray diffraction pattern of $NiCo_2S_4$ NSAs scratched from carbon cloth. The diffraction peaks at 31.6°, 38.3°, 47.4°, 50.5° and 55.3° are attributed to the 311, 400, 422, 511 and 440 planes of the cubic phase $NiCo_2S_4$, respectively. No other diffraction peaks were observed, verifying the formation of phase-pure $NiCo_2S_4$. A possible mechanism is proposed for the conversion process of NiCo precursor NSAs to 3D-networked and mesoporous $NiCo_2S_4$ NSAs. In the aqueous solution, Na_2S dissolves to form S^{2-} ions that are simultaneously hydrolyzed to generate HS^- and H_2S species. These species serve as the sulfur sources for the ion-exchange reaction that converts NiCo precursor to $NiCo_2S_4$. Three-dimensional-networked NiCo precursor NSAs with abundant empty space allow these sulfur sources to diffuse easily into each nanosheet. Because of the presence of OH^- and O_2^- in the NiCo precursor NSAs, a surface redox reaction takes place on their surfaces to form $NiCo_2S_4$ NSAs. The edges of these $NiCo_2S_4$ NSAs subsequently join to form 3D-networked $NiCo_2S_4$ NSAs.

To give further insight into the morphology and structure of the as-prepared 3D-networked $NiCo_2S_4$ NSA/carbon cloth composites, TEM and high-resolution TEM images are shown in Figure 2. Consistent with the scanning electron microcopy observations, the low-magnification TEM image (Figure 2a) reveals the network structure of $NiCo_2S_4$ nanosheets. Interestingly, the as-synthesized $NiCo_2S_4$ nanosheets have a mesoporous structure with a pore size of ~5 nm (Figure 2b). The high-resolution TEM image in Figure 2c demonstrates the crystalline nature of $NiCo_2S_4$ nanosheets, and the existence of lattice discontinuity patches further verifies their mesoporous structure. As denoted in the figure, the interplanar distances were measured to be 0.33 nm and 0.28 nm, which correspond to the *d*-spacing of (220) and (311) planes, respectively, in cubic $NiCo_2S_4$. Figure 2d presents the energy-dispersive X-ray spectrum (EDX) of the $NiCo_2S_4$ nanosheets, which clearly indicates the presence of Ni, Co and S elements. (The Cu signals originate from the TEM grid.)

The N_2 adsorption/desorption isotherm curve and the corresponding pore size distribution plot in Supplementary Figure S3 demonstrate the porous nature of the as-synthesized $NiCo_2S_4$ nanosheets. The Brunauer–Emmett–Teller surface area of $NiCo_2S_4$ nanosheets was calculated to be 109 m^2 g^{-1}. The porous $NiCo_2S_4$ nanosheets exhibited a pore size distribution ranging from 4 to 8 nm as measured by the Barrett–Joyner–Halenda method, agreeing with the TEM image in Figure 2b. The formation of the mesoporous structure could be due to the replacement of O^{2-} by S^{2-} during sulfurization. In previous work, it was determined that more interfacial bonding exists in mesoporous nanostructures, which not only offer more active sites for Li^+ storage but also facilitate Li^+ transfer, resulting in improved specific capacity.[2,30]

Generally, the large volumetric strain of conventional MS nanostructures during charge/discharge processes can lead to cracking, fracture and electrical disconnect from the current collector. This mechanism has been recognized as one of the major causes for rapid capacity fading in LIBs with MS electrodes.[2,3] In this work, we carried

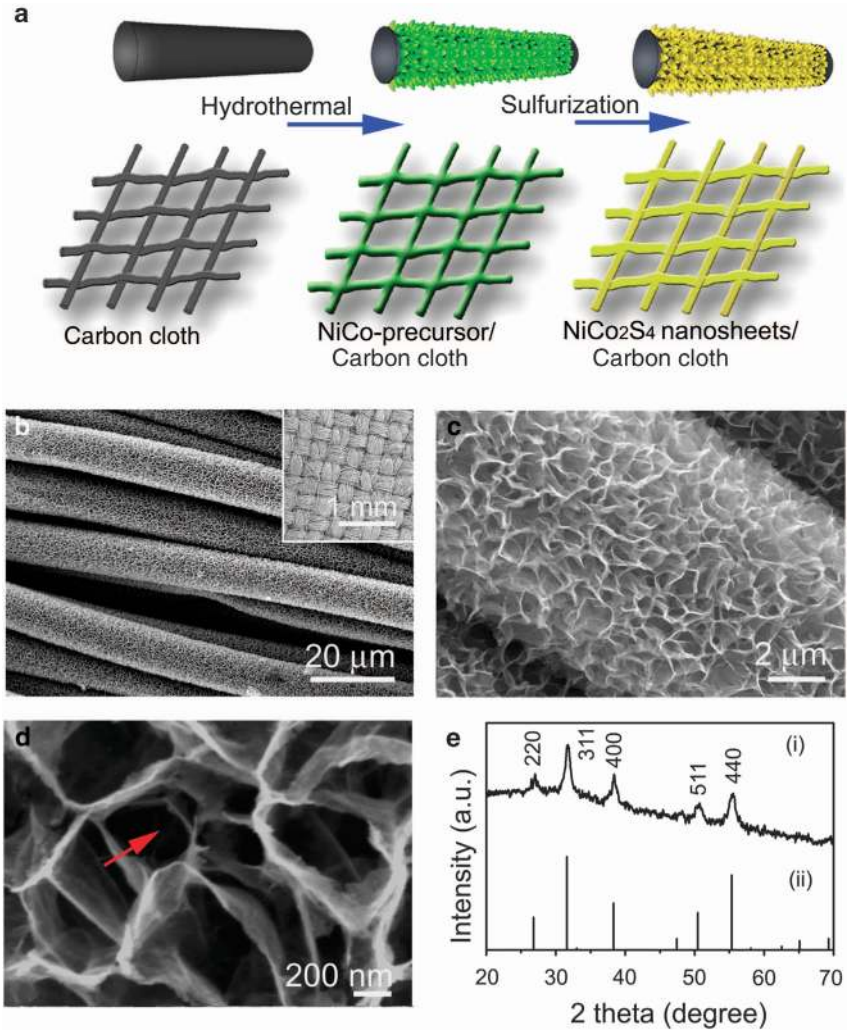

Figure 1 (**a**) Schematic illustration of the synthesis of flexible 3D-networked $NiCo_2S_4$ NSA/carbon cloth through hydrothermal reaction and subsequent sulfurization treatment. (**b**–**d**) SEM images of the $NiCo_2S_4$ NSA/carbon cloth obtained at different magnifications; the inset in **b** shows an SEM image of $NiCo_2S_4$ NSA/carbon cloth at low magnification. (**e**) XRD spectrum of $NiCo_2S_4$ nanosheets scratched from carbon cloth (i) and standard pattern from JCPDS card (No. 20-0782) (ii). NSA, nanosheet array; SEM, scanning electron microcopy; XRD, X-ray diffraction; 3D, three-dimensional.

out *in situ* TEM experiments to investigate mechanical strain in $NiCo_2S_4$ nanosheets during their reaction with Li ions using a dual-probe biasing TEM holder (Nanofactory Instrument).[31,32] The configuration for *in situ* TEM measurements is shown schematically in Figure 3a. $NiCo_2S_4$ nanosheets were decorated on the Cu wire probe, and a small piece of Li/Li_2O was attached to the tip of the opposite W wire probe. By manipulating a piezoelectric motor on the TEM holder, a $NiCo_2S_4$ nanosheet was placed in contact with the lithium oxide and a bias voltage of -3 V was applied to drive Li ions through the solid-state electrolyte (Li_2O) toward the $NiCo_2S_4$ nanosheet.

Figure 3b depicts pristine $NiCo_2S_4$ nanosheets before lithiation. A slight area expansion of the $NiCo_2S_4$ nanosheet was observed after it underwent lithiation for 0.5 min (Figure 3c), and the nanosheet continued to expand with increasing lithiation time, as shown in Supplementary Figure S4. After 20 min (Figure 3d), no further expansion of the nanosheet could be detected, indicating reaction completion. Because the $NiCo_2S_4$ nanosheets have a thickness of ~10 nm, it is challenging to visualize the lithium migration process by *in situ* TEM.[32–34] However, as shown by the selected area electron diffraction patterns (inserts in Figures 3b and d), the conversion of the $NiCo_2S_4$ nanosheet from its original crystalline phase to an amorphous phase after 20 min can be considered indirect evidence of the lithiation process. Moreover, the detectable expansion of the $NiCo_2S_4$ nanosheet itself indicates that lithiation occurred. In this work, the volumetric expansion was estimated by measuring the area increase of the nanosheet in the TEM images depicted in Figures 3b and d. An area increase of ~37% was obtained after lithiation for 20 min. If we assume that expansion is isotropic, the volumetric expansion of $NiCo_2S_4$ nanosheet can be estimated to be ~60%. Interestingly, the $NiCo_2S_4$ nanosheet displayed no cracking or fracture as a result of the lithiation process. The existence of the large quantity of mesopores in $NiCo_2S_4$ nanosheets compensated for the volumetric expansion during the lithiation process; consequently, changes in the dimensions and morphology of nanosheets were negligible, and the nanosheets retained their mechanical integrity.

The electrochemical properties of the 3D-networked $NiCo_2S_4$ NSA/carbon cloth composite as an anode material for LIB were evaluated. Figure 4a displays representative cyclic voltammetry (CV) for the first, second and fifth cycles at a scan rate of 1 mV s^{-1} in the voltage

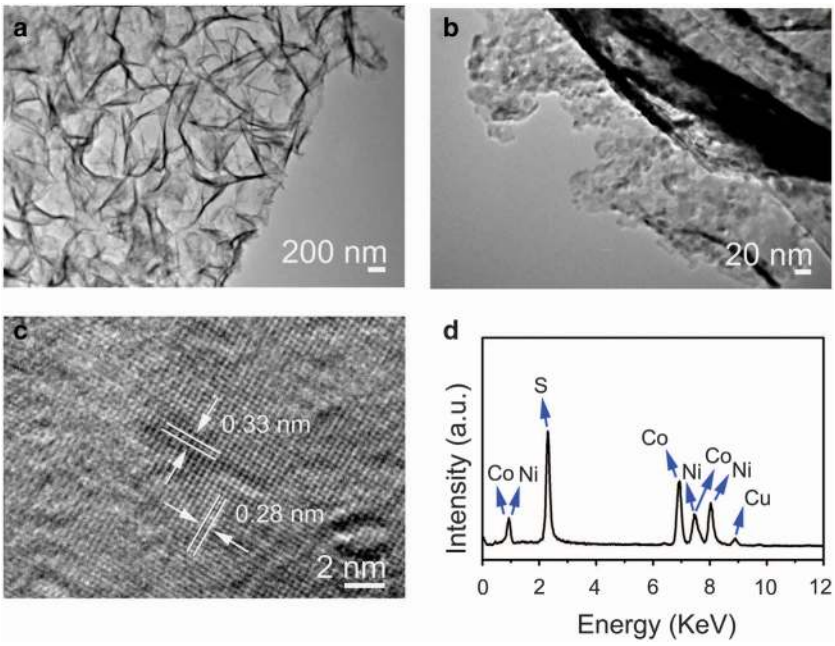

Figure 2 (**a** and **b**) TEM images of $NiCo_2S_4$ nanosheets at different magnifications. (**c**) HRTEM image of $NiCo_2S_4$ nanosheets. (**d**) Representative EDX spectrum of $NiCo_2S_4$ nanosheets scratched from carbon cloth. HRTEM, high-resolution TEM; TEM, transmission electron microscopy; EDX, energy-dispersive X-ray spectroscopy.

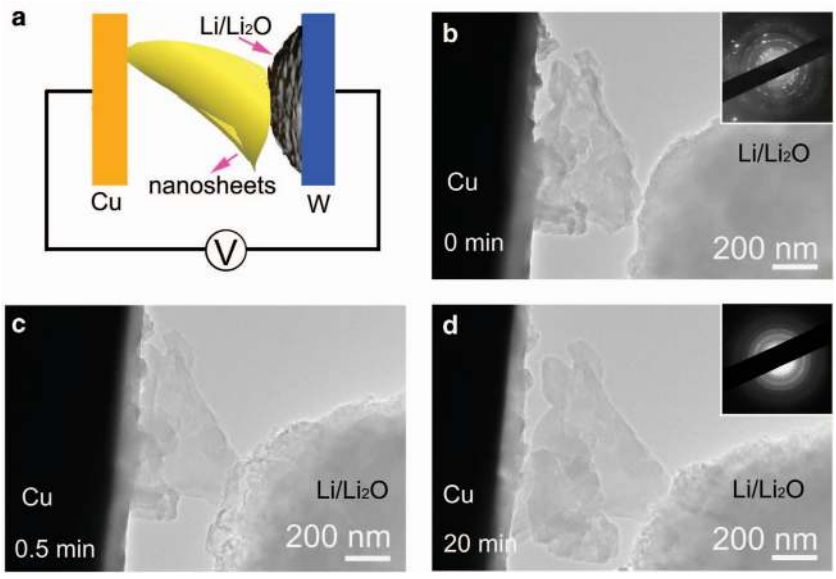

Figure 3 (**a**) Schematic showing the configuration for *in situ* TEM observation of the lithiation process. A $NiCo_2S_4$ nanosheet was placed on a Cu wire, serving as the working electrode; the counter-electrode consisted of a small piece of Li metal coated with Li_2O (solid electrolyte) on the tip of a W wire. A bias voltage of −3 V was applied between the two electrodes to drive the lithiation process. (**b**–**d**) TEM images monitoring the lithiation process of $NiCo_2S_4$ nanosheet at time equal to 0, 0.5 and 20 min, respectively. The insets in **b** and **d** show the corresponding SAED patterns of the $NiCo_2S_4$ nanosheet. SAED, selected area electron diffraction; TEM, transmission electron microscopy.

window of 0.01–3 V vs Li/Li^+. To distinguish the oxidation and reduction reactions induced by the $NiCo_2S_4$ NSAs, the electrochemical characteristics of pure carbon cloth were studied under the same testing conditions, as shown in Supplementary Figure S5. By comparing the CV curves of pure carbon cloth and 3D-networked $NiCo_2S_4$ NSA/carbon cloth, the dominant irreversible cathodic peak of $NiCo_2S_4$ NSAs, which was located at ~1.1 V in the first cathodic sweep, could be assigned to the reduction of Ni^{2+} and Co^{3+} into metallic Ni and Co, respectively.[35] Furthermore, the peaks at ~1.4 and 2.0 V in the subsequent anodic scan could be ascribed to oxidation of metallic Ni and Co to NiS_x and CoS_x, respectively. In subsequent cycles, the main cathodic peaks shifted toward a higher potential and the anodic peaks downshifted slightly. The upshift and intensity decrease of the main cathodic peak are due to the occurrence of

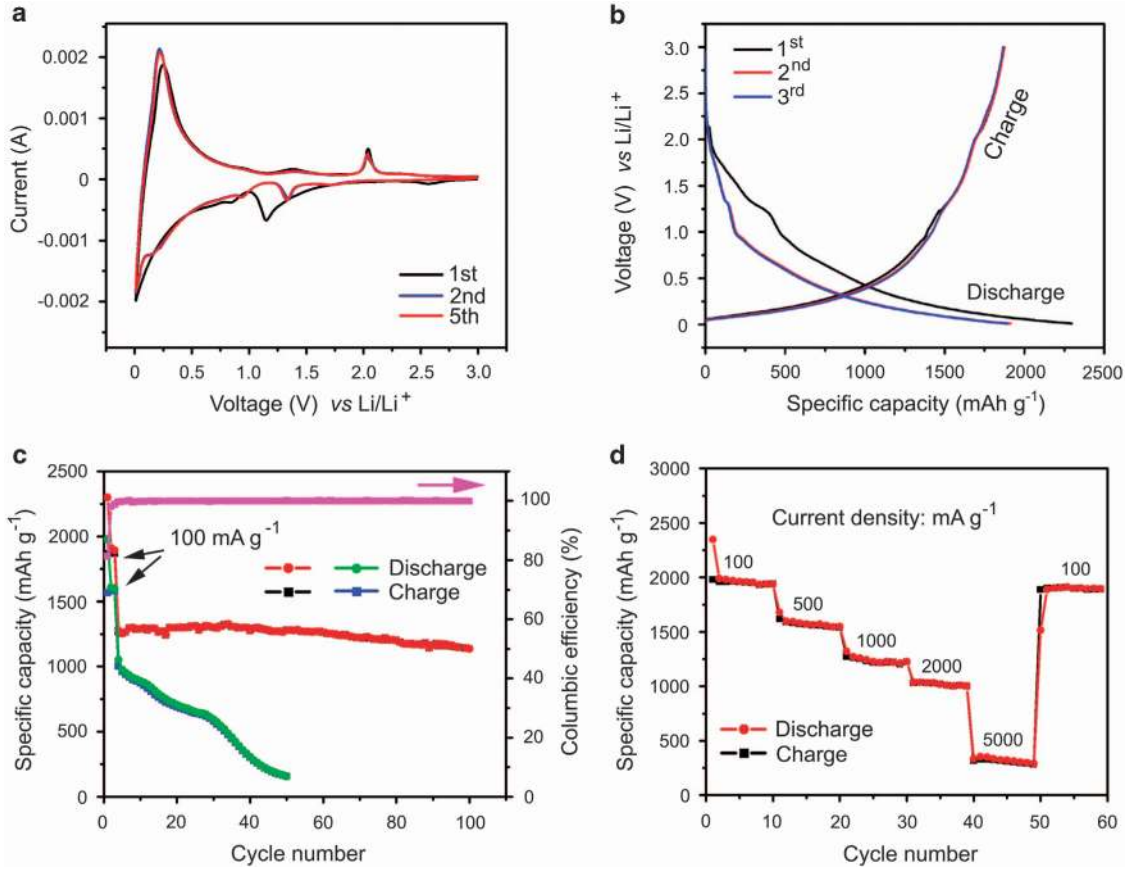

Figure 4 (**a**) CV curves of 3D-networked $NiCo_2S_4$ NSA/carbon cloth obtained at a scan rate of 0.1 mV s^{-1} between 0.01 and 3 V. (**b**) Charge–discharge curves of 3D-networked $NiCo_2S_4$ NSA/carbon cloth at a constant current density of 100 mA g^{-1}. (**c**) Cycling performance and corresponding Coulombic efficiency of 3D-networked $NiCo_2S_4$ NSA/carbon cloth measured at 1000 mA g^{-1}. The cycling performance of $NiCo_2S_4$ flowers electrodes is also presented. (**d**) Rate performance of 3D-networked $NiCo_2S_4$ NSA/carbon cloth electrode at various current densities. NSA, nanosheet array; 3D, three-dimensional.

certain irreversible reactions associated with the formation of a solid electrolyte interphase (SEI) film on the electrode surface.[36] The overlap in CV curves after the second cycle indicates good reversibility of the electrochemical reactions. Figure 4b shows the galvanostatic discharge/charge profiles of the 3D-networked $NiCo_2S_4$ NSA/carbon cloth electrodes at a current density of 100 mA g^{-1} for the first three cycles. The first cycle reveals discharge and charge capacities of 2298 mAh g^{-1} and 1868 mAh g^{-1}, respectively, indicating an initial Coulombic efficiency of 81.2%. The irreversible capacity loss for the first cycle can be attributed to the formation of an SEI layer and possible incomplete restoration of metallic Ni and Co into the original sulfide, an effect that has been commonly observed in $NiCo_2O_4$ electrode materials.[22,35] In the second and third cycles, the discharge capacities of the electrode decreased to 1912 mAh g^{-1} and 1891 mAh g^{-1}, respectively, and the corresponding Coulombic efficiency increased to 98.1% and 98.8%, respectively. The sharp increase in Coulombic efficiency indicates that a stable SEI layer had already formed during the initial cycles.

The cycling stability of the $NiCo_2S_4$ NSA/carbon cloth electrodes was tested by performing discharge-charge measurements up to 100 cycles, as shown in Figure 4c. Note that the test was performed at the low rate of 100 mA g^{-1} for the first three cycles to enable the slow activation of $NiCo_2S_4$ NSAs and the development of a stable SEI layer; the current density was subsequently increased to 1000 mA g^{-1}. The discharge capacity was 1275 mAh g^{-1} for the fourth cycle and 1137 mAh g^{-1} after 100 cycles, corresponding to a capacity retention of 89.2% (red and black represent the discharge and charge curves, respectively), which is higher than that of previously reported MS nanostructures and MS composite electrodes.[12–15,18–21,37–39] In addition, the Columbic efficiency increased sharply from 81.2% for the first cycle to >99.8% after several initial cycles, and then stayed at this level until the 100 cycles were completed. The extremely high columbic efficiency indicates that a stable SEI layer formed during the initial cycles. The stability test was also performed at an elevated current density of 2000 mA g^{-1} (Supplementary Figure S6), at which the electrode was capable of delivering a high discharge capacity of 792 mAh g^{-1} after 100 cycles, retaining 68.4% of the fourth-cycle discharge capacity of 1158 mAh g^{-1}. Significantly, a high Coulombic efficiency (>99.6%, except for the first few cycles) was also achieved. Notably, the corresponding capacity and stability evaluations of the carbon-only cloth electrode (Supplementary Figure S7) verified the negligible contribution of carbon cloth to the overall capacity of $NiCo_2S_4$ NSA/carbon cloth electrodes (~17 out of 1275 mAh g^{-1}).

As a control sample, pure $NiCo_2S_4$ flower nanostructures were synthesized (Supplementary Figure S8), and their cyclic stability as electrodes was also tested at 1000 mA g^{-1}, as shown in Figure 4c (green and blue curves represent discharge and charge curves, respectively). The electrode was fabricated in a conventional way by mixing the $NiCo_2S_4$ flowers with binder and conductive carbon. In sharp contrast to the $NiCo_2S_4$ NSA/carbon cloth electrodes, the

capacity of the $NiCo_2S_4$ flower electrode declined considerably from ~1050 mAh g^{-1} during the fourth cycle to 159 mAh g^{-1} after 50 cycles. Moreover, the Coulombic efficiency of the cell was only 96–98% (except for the first three cycles), indicating its low electrochemical reversibility (Supplementary Figure S9). The low Coulombic efficiency could be an indication of SEI layer instability, which is closely related to lithiation-induced capacity degradation.[8] The results summarized above clearly demonstrate the superiority of 3D-networked $NiCo_2S_4$ NSA/carbon cloth for use as LIB anodes.

The rate performance of the 3D-networked $NiCo_2S_4$ NSA/carbon cloth electrodes was further studied by cycling at different current densities. As shown in Figure 4d, capacity decreased from 1950 to 1560, 1220, 1030 and 340 mAh g^{-1} when the current density was increased from 100 to 500 mA g^{-1}, 1000 mA g^{-1}, 2000 mA g^{-1}, and 5000 mA g^{-1}, respectively. Notably, a capacity of 340 mAh g^{-1} was retained at the relatively high current density of 5000 mA g^{-1}, a value comparable to the theoretical capacity of carbon/graphite-based electrodes (372 mAh g^{-1}),[40] illustrating the high rate capability of 3D-networked $NiCo_2S_4$ NSA/carbon cloth. After cycling at the highest current density of 5000 mA g^{-1}, the capacity recovered was ~1900 mAh g^{-1} as the current density was switched back to 100 mA g^{-1}, corresponding to a capacity retention of ~97%, which indicates high stability as well as excellent reversibility of the electrode.

To characterize $NiCo_2S_4$ NSAs grown directly on carbon cloth, we collected electrochemical impedance spectra of the electrodes made of 3D-networked $NiCo_2S_4$ NSA/carbon cloth and $NiCo_2S_4$ flowers, as shown in Figure 5a. The Nyquist plots of each sample depict a semicircle in the high-to-medium frequency region and an inclined line in the low frequency region. The semicircle is attributed to the charge transfer process at the electrode/electrolyte interface, and the inclined line corresponds to lithium diffusion, or Warburg diffusion, into the bulk of the electrode. The modified equivalent circuit model of the system is provided in Figure 5b.[41–43] The parameter Rs is the electrolyte resistance; CPE1 and R_f are the capacitance and resistance, respectively, of the passivation SEI film formed on the electrode surface; CPE2 and R_{ct} are the double-layer capacitance and charge transfer resistance, respectively; and Zw is the Warburg impedance related to the diffusion of lithium ions into the bulk of the electrode. For the $NiCo_2S_4$ NSA/carbon cloth electrode, the fitted impedance parameters were $R_f = 17.42\ \Omega$, and $R_{ct} = 81.75\ \Omega$; for the $NiCo_2S_4$ flower electrode, $R_f = 54.11\ \Omega$ and $R_{ct} = 96.79\ \Omega$. It is obvious that R_f and R_{ct} for the $NiCo_2S_4$ NSA/carbon cloth electrode are significantly lower than those of the $NiCo_2S_4$ flower electrode. Therefore, the 3D-networked $NiCo_2S_4$ NSAs enable rapid electron transport and fast faradic reaction during electrochemical lithium insertion/extraction processes.

Binder and conductive carbon are used in the $NiCo_2S_4$ flower electrode; the electroactive materials thus present considerable resistance to electron transport to and from the current collector substrate, as illustrated schematically in Figure 5c. Such particulate nanostructures have also been demonstrated to have a tendency during cycling to aggregate and form disconnected clusters that may further deteriorate electron conduction between the active materials and the current collector.[44] Moreover, it is less likely that an electrode consisting of binder and conductive carbon can provide a large and effective contact area between the active material and the electrolyte, maintain a short diffusion distance for Li^+ or suitably accommodate mechanical strain during cycling.[45] In comparison with the $NiCo_2S_4$ flower electrode, the 3D-networked $NiCo_2S_4$ NSA/carbon cloth electrode possesses the following merits: (1) $NiCo_2S_4$ has inherently high electronic conductivity (~4 orders of magnitude higher than that of conventional MO semiconductors); and the nanosheets are anchored tightly to the (carbon fiber) current collector, forming good electrical contact. Moreover, the hybrid structure can be used directly as an anode without the addition of binders and conductive carbon, as illustrated in Figure 5d. Thus, it can facilitate fast Li^+ ion and electron kinetics during the redox reaction, leading to high capacity and outstanding cycling stability. (2) Because of their mesoporous nature, $NiCo_2S_4$ nanosheets exhibit relatively small volumetric expansion during the lithiation process, as the existence of voids in the NSAs (Figure 1d) provides sufficient free space to ameliorate the tendency for expansion. Furthermore, the robust 3D interpenetrating network structure can withstand the strain induced by volumetric changes during electrochemical reactions and can thus maintain the integrity of the hybrid, leading to increased cycling stability during lithiation/delithiation processes. (3) The enlarged surface area of the ultrathin and mesoporous $NiCo_2S_4$ nanosheets and their 3D network assembly greatly enhances the electrolyte/active material contact area, which

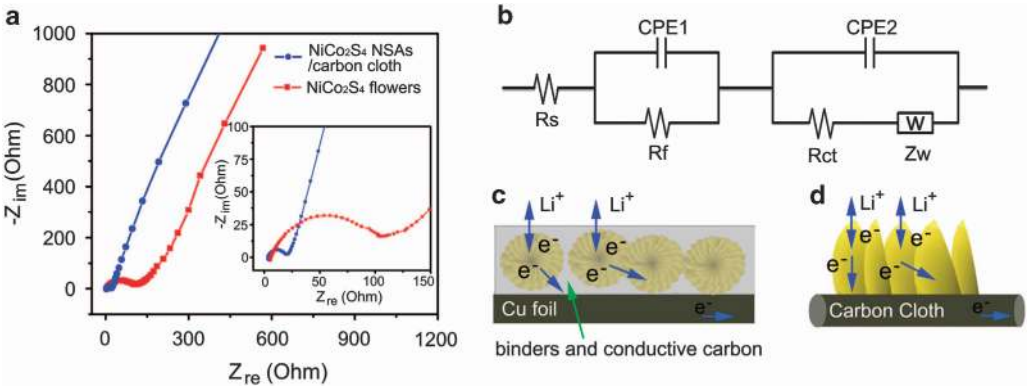

Figure 5 (**a**) Nyquist plots of the 3D-networked $NiCo_2S_4$ NSA/carbon cloth and $NiCo_2S_4$ flower electrodes measured at an amplitude of 5 mV over a frequency range from 100 kHz to 0.01 Hz; the inset is the magnified view in the high-frequency region. (**b**) Equivalent circuit model of $NiCo_2S_4$ NSA/carbon cloth and $NiCo_2S_4$ flower electrodes. Schematic diagrams showing the transport of electrons and Li ions in electrodes containing (**c**) $NiCo_2S_4$ flowers and (**d**) 3D-networked $NiCo_2S_4$ NSA/carbon cloth. Three-dimensional-networked $NiCo_2S_4$ nanosheet array/carbon cloth composites are synthesized by a simple hydrothermal reaction and subsequent sulfurization process, and the rational design of their material composition and structure leads to outstanding overall performance as an anode material in lithium-ion batteries. NSA, nanosheet array; 3D, three-dimensional.

may facilitate electrolyte penetration and the transport of lithium ions. Thus, in a synergistic manner resulting from their 3D assembly, the nanosheets not only act as reservoirs for storage of Li^+ ions but also reduce the transport length of Li^+ ions, which improves specific capacity. The unique material composition, morphology and structure of the 3D-networked $NiCo_2S_4$ NSA/carbon cloth electrodes lead to their outstanding specific capacity, excellent cycling stability and high rate performance.

CONCLUSIONS

In summary, 3D-networked $NiCo_2S_4$ NSAs were successfully grown on carbon cloth substrates through a surfactant-assisted hydrothermal method combined with a simple sulfurization treatment. $NiCo_2S_4$ has inherently high electronic conductivity, and the $NiCo_2S_4$ NSA/carbon cloth hybrid can be directly employed as a high-performance electrode for LIBs without the addition of binders or conducting materials. Significantly, the $NiCo_2S_4$ nanosheets were found to exhibit only slight volumetric expansion (~60%) during the lithiation process as a result of their mesoporous nature. In addition, the 3D network structure and void space of $NiCo_2S_4$ nanosheets are expected to provide structural robustness, efficient electron transfer, fast ion transport, large surface area and easy access of electrolyte to electrode. As an anode material in LIBs, the $NiCo_2S_4$ NSA/carbon cloth hybrid delivered high specific capacity, excellent cycling stability and outstanding rate performance. At a current density of 1000 mA g^{-1}, the relatively large capacity of 1275 mAh g^{-1} was demonstrated; this value decreased only minimally to 1137 mAh g^{-1} after 100 cycles. Even at the high current density of 5000 mA g^{-1}, the composite material exhibited a capacity of 340 mAh g^{-1}, which is comparable to the theoretical capacity of carbon/graphite-based electrodes. The outstanding overall properties of the 3D-networked $NiCo_2S_4$ NSA/carbon cloth hybrid make it a promising anode material candidate for high-performance LIBs.

CONFLICT OF INTEREST

The authors declare no conflict of interest.

ACKNOWLEDGEMENTS

This work was financially supported by the Applied Research Grant of the City University of Hong Kong (ARG 9667111), the National Natural Science Foundation of China (Grant Nos. 21171035, 51302035 and 51372213), the PhD Programs Foundation of the Ministry of Education of China (No. 20130075120001 and 20110075110008), the China Postdoctoral Science Foundation (2014M550203), the Science and Technology Commission of Shanghai Municipality (Grant No. 13ZR1451200) and the Fundamental Research Funds for the Central Universities (Grant No. 2232013D3-09).

1 McDowell, M. T., Lee, S. W., Nix, W. D. & Cui, Y. Understanding the lithiation of silicon and other alloying anodes for lithium-ion batteries. *Adv. Mater.* **25**, 4966–4985 (2013).
2 Armstrong, M. J., O'Dwyer, C., Macklin, W. J. & Holmes, J. D. Evaluating the performance of nanostructured materials as lithium-ion battery electrodes. *Nano Res.* **7**, 1–62 (2014).
3 Zhu, J. X., Yang, D., Yin, Z. Y., Yan, Q. Y. & Zhang, H. Graphene and graphene-based materials for energy storage applications. *Small* **10**, 3480–3498 (2014).
4 Liu, N., Lu, Z. D., Zhao, J., McDowell, M. T., Lee, H. W., Zhao, W. T. & Cui, Y. A pomegranate-inspired nanoscale design for large-volume-change lithium battery anodes. *Nat. Nanotechnol.* **9**, 187–192 (2014).
5 Cao, X. H., Shi, Y. M., Shi, W. H., Rui, X. H., Yan, Q. Y., Kong, J. & Zhang, H. Preparation of MoS2-coated three-dimensional graphene networks for high-performance anode material in lithium-ion batteries. *Small* **9**, 3433–3438 (2013).
6 Zhang, G. Q., Xia, B. Y., Xiao, C., Yu, L., Wang, X., Xie, Y. & Lou, X. W. General formation of complex tubular nanostructures of metal oxides for the oxygen reduction reaction and lithium-ion batteries. *Angew. Chem. Int. Ed.* **52**, 8643–8647 (2013).
7 Zhao, Y. L., Feng, J. G., Liu, X., Wang, F. C., Wang, L. F., Shi, C. W., Huang, L., Feng, X., Chen, X. Y., Xu, L., Yan, M. Y., Zhang, Q., Bai, X. D., Wu, H. G. & Mai, L. Q. Self-adaptive strain-relaxation optimization for high-energy lithium storage material through crumpling of graphene. *Nat. Commun.* **5**, 4565 (2014).
8 Sun, H. T., Xin, G. Q., Hu, T., Yu, M. P., Shao, D. L., Sun, X. & Lian, J. High-rate lithiation-induced reactivation of mesoporous hollow spheres for long-lived lithium-ion batteries. *Nat. Commun.* **5**, 4526 (2014).
9 Zhang, L., Wu, H. B., Liu, B. & Lou, X. W. Formation of porous SnO2 microboxes via selective leaching for highly reversible lithium storage. *Energy Environ. Sci.* **7**, 1013–1017 (2014).
10 Zhu, J. X., Yin, Z. Y., Yang, D., Sun, T., Yu, H., Hoster, H. E., Hng, H. H., Zhang, H. & Yan, Q. Y. Hierarchical hollow spheres composed of ultrathin Fe2O3 nanosheets for lithium storage and photocatalytic water oxidation. *Energy Environ. Sci.* **6**, 987–993 (2013).
11 Chao, D. L., Xia, X. H., Liu, J. L., Fan, Z. X., Ng, C. F., Lin, J. Y., Zhang, H., Shen, Z. X. & Fan, H. J. A V2O5/conductive-polymer core/shell nanobelt array on three-dimensional graphite foam: a high-rate, ultrastable, and freestanding cathode for lithium-ion batteries. *Adv. Mater.* **26**, 5794–5800 (2014).
12 Liu, J., Wen, Y. R., Wang, Y., van Aken, P. A., Maier, J. & Yu, Y. Carbon-encapsulated pyrite as stable and earth-abundant high energy cathode material for rechargeable lithium batteries. *Adv. Mater.* **26**, 6025–6030 (2014).
13 Mahmood, N., Zhang, C. & Hou, Y. Nickel sulfide/nitrogen-doped graphene composites: phase-controlled synthesis and high performance anode materials for lithium-ion batteries. *Small* **9**, 1321–1328 (2013).
14 Wan, Z. M., Shao, J., Yun, J. J., Zheng, H. Y., Gao, T., Shen, M., Qu, Q. T. & Zheng, H. H. Core-shell structure of hierarchical quasi-hollow MoS2 microspheres encapsulated porous carbon as stable anode for Li-ion batteries. *Small* **10**, 4975–4981 (2014).
15 Shiva, K., Matte, H. S. S. R., Rajendra, H. B., Bhattacharyya, A. J. & Rao, C. N. R. Employing synergistic interactions between few-layer WS2 and reduced graphene oxide to improve lithium storage, cyclability and rate capability of Li-ion batteries. *Nano Energy* **2**, 787–793 (2013).
16 Ji, L. W., Lin, Z., Alcoutlabi, M. & Zhang, X. G. Recent developments in nanostructured anode materials for rechargeable lithium-ion batteries. *Energy Environ. Sci.* **4**, 2682–2699 (2011).
17 Rui, X. H., Tan, H. T. & Yan, Q. Y. Nanostructured metal sulfides for energy storage. *Nanoscale* **6**, 9889–9924 (2014).
18 Wang, Y. M., Wu, J. J., Tang, Y. F., Lu, X. J., Yang, C. Y., Qin, M. S., Huang, F. Q., Li, X. & Zhang, X. Phase-controlled synthesis of cobalt sulfides for lithium ion batteries. *ACS Appl. Mater. Interfaces* **4**, 4246–4250 (2012).
19 Wang, C., Wan, W., Huang, Y. H., Chen, J. T., Zhou, H. H. & Zhang, X. X. Hierarchical MoS2 nanosheet/active carbon fiber cloth as a binder-free and free-standing anode for lithium-ion batteries. *Nanoscale* **6**, 5351–5358 (2014).
20 Lai, C. H., Huang, K. W., Cheng, J. H., Lee, C. Y., Lee, W. F., Huang, C. T., Hwang, B. J. & Chen, L. J. Oriented growth of large-scale nickel sulfide nanowire arrays via a general solution route for lithium-ion battery cathode applications. *J. Mater. Chem.* **19**, 7277–7283 (2009).
21 Cai, R., Chen, J., Zhu, J. X., Xu, C., Zhang, W. Y., Zhang, C. M., Shi, W. H., Tan, H. T., Yang, D., Hng, H. H., Lim, T. M. & Yan, Q. Y. Synthesis of CuxS/Cu nanotubes and their lithium storage properties. *J. Phys. Chem. C* **116**, 12468–12474 (2012).
22 Shen, L. F., Che, Q., Li, H. G. & Zhang, X. G. Mesoporous NiCo2O4 nanowire arrays grown on carbon textiles as binder-free flexible electrodes for energy storage. *Adv. Funct. Mater.* **24**, 2630–2637 (2014).
23 Liu, B., Zhang, J., Wang, X. F., Chen, G., Chen, D., Zhou, C. W. & Shen, G. Z. Hierarchical three-dimensional ZnCo2O4 nanowire arrays/carbon cloth anodes for a novel class of high-performance flexible lithium-ion batteries. *Nano Lett.* **12**, 3005–3011 (2012).
24 Hu, C. G., Zhai, X. Q., Liu, L. L., Zhao, Y., Jiang, L. & Qu, L. T. Spontaneous reduction and assembly of graphene oxide into three-dimensional graphene network on arbitrary conductive substrates. *Sci. Rep.* **3**, 2065 (2013).
25 Lee, S. K., Song, M. J., Kim, J. H., Kan, T. S., Lim, Y. K., Ahn, J. P. & Lim, D. S. 3D-networked carbon nanotube/diamond core-shell nanowires for enhanced electrochemical performance. *NPG Asia Mater.* **6**, e115 (2014).
26 Chen, H. C., Jiang, J. J., Zhang, L., Wan, H. Z., Qi, T. & Xia, D. D. Highly conductive NiCo2S4 urchin-like nanostructures for high-rate pseudocapacitors. *Nanoscale* **5**, 8879–8883 (2013).
27 Xiao, J. W., Wan, L., Yang, S. H., Xiao, F. & Wang, S. A. Design hierarchical electrodes with highly conductive NiCo2S4 nanotube arrays grown on carbon fiber paper for high-performance pseudocapacitors. *Nano Lett.* **14**, 831–838 (2014).
28 Yu, L., Zhang, L., Wu, H. B. & Lou, X. W. Formation of NixCo3-xS4 hollow nanoprisms with enhanced pseudocapacitive properties. *Angew. Chem. Int. Ed.* **53**, 3711–3714 (2014).
29 Luo, J. S., Xia, X. H., Luo, Y. S., Guan, C., Liu, J. L., Qi, X. Y., Ng, C. F., Yu, T., Zhang, H. & Fan, H. J. Rationally designed hierarchical TiO2@Fe2O3 hollow nanostructures for improved lithium ion storage. *Adv. Energy Mater.* **3**, 737–743 (2013).
30 Zhang, Q. B., Chen, H. X., Wang, J. X., Xu, D. G., Li, X. H., Yang, Y. & Zhang, K. L. Growth of hierarchical 3D mesoporous NiSix/NiCo2O4 core/shell heterostructures on nickel foam for lithium-ion batteries. *ChemSusChem* **7**, 2325–2334 (2014).
31 Zou, R. J., Zhang, Z. Y., Liu, Q., Xu, K. B., Lu, A. J., Hu, J. Q., Li, Q., Bando, Y. & Golberg, D. Melting of metallic electrodes and their flowing through a carbon nanotube channel within a device. *Adv. Mater.* **25**, 2693–2699 (2013).

32 Liu, X. H., Liu, Y., Kushima, A., Zhang, S. L., Zhu, T., Li, J. & Huang, J. Y. *In situ* TEM experiments of electrochemical lithiation and delithiation of individual nanostructures. *Adv. Energy Mater.* **2**, 722–741 (2012).
33 Zheng, G. Y., Lee, S. W., Liang, Z., Lee, H. W., Yan, K., Yao, H. B., Wang, H. T., Li, W. Y., Chu, S. & Cui, Y. Interconnected hollow carbon nanospheres for stable lithium metal anodes. *Nat. Nanotechnol.* **9**, 618–623 (2014).
34 Su, Q. M., Xie, J., Zhang, J., Zhong, Y. J., Du, G. H. & Xu, B. S. *In situ* transmission electron microscopy observation of electrochemical behavior of CoS2 in lithium-ion battery. *ACS Appl. Mater. Interfaces* **6**, 3016–3022 (2014).
35 Gao, G. X., Wu, H. B. & Lou, X. W. Citrate-assisted growth of NiCo2O4 nanosheets on reduced graphene oxides for highly reversible lithium storage. *Adv. Energy Mater.* **4**, 1400422 (2014).
36 Wang, R. H., Xu, C. H., Sun, J., Liu, Y. Q., Gao, L., Yao, H. L. & Lin, C. H. Heat-induced formation of porous and free-standing MoS2/GS hybrid electrodes for binder-free and ultralong-life lithium ion batteries. *Nano Energy* **8**, 183–195 (2014).
37 Zhang, L., Zhou, L., Wu, H. B., Xu, R. & Lou, X. W. Unusual formation of single-crystal manganese sulfide microboxes co-mediated by the cubic crystal structure and shape. Angew. *Angew. Chem. Int. Ed.* **51**, 7267–7270 (2012).
38 Ni, J. F., Zhao, Y., Liu, T. T., Zheng, H. H., Gao, L. J., Yan, C. L. & Li, L. Strongly coupled Bi2S3@CNT hybrids for robust lithium storage. *Adv. Energy Mater.* **4**, 1400798 (2014).
39 Zhou, T. F., Pang, W. K., Zhang, C. F., Yang, J. P., Chen, Z. X., Liu, H. K. & Guo, Z. P. Enhanced sodium-ion battery performance by structural phase transition from two-dimensional hexagonal-SnS2 to orthorhombic-SnS. *ACS Nano* **8**, 8323–8333 (2014).
40 Tang, J. J., Chen, G. G., Yang, J., Zhou, X. Y., Zhou, L. M. & Huang, B. Silica-assistant synthesis of three-dimensional graphene architecture and its application as anode material for lithium ion batteries. *Nano Energy* **8**, 62–72 (2014).
41 Jiang, H., Hu, Y. J., Guo, S. J., Yan, C. Y., Lee, P. S. & Li, C. Z. Rational design of MnO/carbon nanopeapods with internal void space for high-rate and long-life Li-ion batteries. *ACS Nano* **8**, 6038–6046 (2014).
42 Wang, L. Y., Zhuo, L. H., Cheng, H. Y., Zhang, C. & Zhao, F. Y. Porous carbon nanotubes decorated with nanosized cobalt ferrite as anode materials for high-performance lithium-ion batteries. *J. Power Sources* **283**, 289–299 (2015).
43 Klink, S., Höche, D., Mantia, F. L. & Schuhmann, W. FEM modelling of a coaxial three-electrode test cell for electrochemical impedance spectroscopy in lithium ion batteries. *J. Power Sources* **283**, 273–280 (2013).
44 Tang, Y. X., Zhang, Y. Y., Deng, J. Y., Wei, J. Q., Tam, H. L., Chandran, B. K., Dong, Z. L., Chen, Z. & Chen, X. D. Mechanical force-driven growth of elongated bending TiO2-based nanotubular materials for ultrafast rechargeable lithium ion batteries. *Adv. Mater.* **26**, 6111–6118 (2014).
45 Liu, H., Bi, Z., Sun, X. G., Unocic, R. R., Paranthaman, M. P., Dai, S. & Brown, G. M. Mesoporous TiO2-B microspheres with superior rate performance for lithium ion batteries. *Adv. Mater.* **23**, 3450–3454 (2011).

Supplementary Information accompanies the paper on the NPG Asia Materials website (http://www.nature.com/am)